A NEW APPROACH FOR THE INVESTIGATION OF THE FLUID FLOW IN CERAMIC FOAM FILTERS

Bettina Hübschen[1]; Joachim G. Krüger[1]; Neil J. Keegan[2]; Wolfgang Schneider[3]
[1]RWTH Aachen, Aachen Germany
[2]Pyrotek Engineering Materials Limited, Dudley UK
[3]VAW aluminium AG, Bonn Germany

Abstract
The filtration efficiency of ceramic foam filters depends strongly on the fluid flow in the channels of the filters. To investigate this, two new water models were used. The first one was a full scale filter box model. Tracer tests on the CFF were made to investigate the change of flow behaviour with the flow rate and filter pore size. The transient point from laminar to turbulent flow could be determined by pressure drop measurements. The second water model used was a specially designed single channel model to simulate the flow in one channel of a CFF. By pulse input of a tracer, the flow behaviour could be determined quantitatively. It was found that flow velocity is a crucial parameter for filtration efficiency. Filtration volume decreases rapidly if filtration velocity increases, thus making deposition of particles more unlikely.

Introduction
Pyrotek Engineering Materials Ltd, UK, VAW aluminium AG, Germany and RWTH Aachen, Department of nonferrous process metallurgy, Germany, decided to start together fundamental research about liquid metal filtration to get a better understanding for this phenomenon.
Deep bed filtration is considered as the dominant filtration mode for ceramic foam filters operating at the cleanliness levels existing in aluminium plants today [1]
In deep bed filtration of molten metal the inclusions, which are generally smaller than the pore sizes of the filter typically used, are only deposited on the pore walls and can therefore be carried away with the liquid metal during hydrodynamic perturbations [2]. Inclusion capture in deep bed filtration is considered to be a result of two sequential events:

- transport of an inclusion to capture sites on the filter media
- attachment of the particles to these sites [3]

In general, *particle transport* can occur by impingement, interception, sedimentation, diffusional, and hydrodynamic effects. When the difference in density is high, the sedimentation forces will play an important role. If the difference decreases, sedimentation will become negligible and interception will become the dominant factor.

Particle attachment can be a result of forces developed through pressure, chemical, or van der Waals effects.

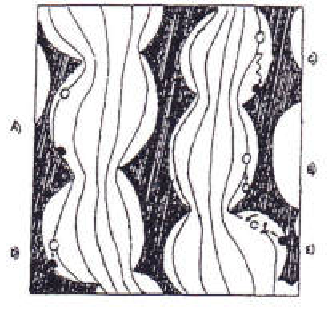

Figure 1: Transport mechanisms of a particle in deep bed filtration [4] A) direct interception B) gravity forces C) Brownian movement D) Inertial Forces E) Hydrodynamic effects

The relative dominance of each mechanism is a function of *particulate type and size, fluid approach velocity*, as well as *temperature* and *media characteristics*.

The tortuous path of a particle through the filter, coupled with rapid changes in direction and velocity of the molten aluminium, make the probability of impingement quite high. The probability that a particle will be retained is dependant on many variables, such as

- the chemical composition of the particle and filter
- the filter microporosity, topography and wettability
- the velocity (flow rate) of metal through the filter
- the laminar flow characteristics of the molten Aluminium adjacent to a given filter surface area
- the particle size and morphology [5]

If the viscous drag on the particle is not higher than the forces that cause retainment, the inclusion will remain inside the filter.

Considerations about the real velocities in the filter have to be done. As inside the filter the pore size changes, so will the velocity of the melt. This means that there are regions with turbulent flow and such with laminar flow. This change of velocity is especially important as the turbulent flow allows very small particles to agglomerate and then be attached in the regions with laminar flow.

However turbulent flow can lead to the release of already attached particles due to drag forces. It can be expected that the magnitude of the drag forces is proportional to the magnitude of velocity in the viscous flow regime.[6]

This means the fluid flow influences both parts of inclusion capture.

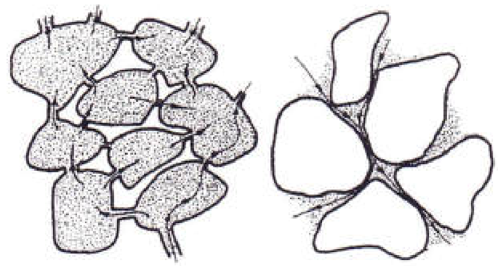

Figure 2: Schematic diagram illustrating the different flow regimes operating in cellular and granular media [7]

The Ceramic Foam Filter forms a cellular media and can be regarded as the negative of a packed bed of granules[6]. Therefore the flow regimes in ceramic foam filters and packed beds are essentially different. Figure 2 shows the different flow regimes in a ceramic foam filter and in a granular media used for drinking water production [7].

Within these pores different flow conditions and mixing behaviour can occur, depending on flow velocity. Figure 3 illustrates the different flow lines inside a single pore.

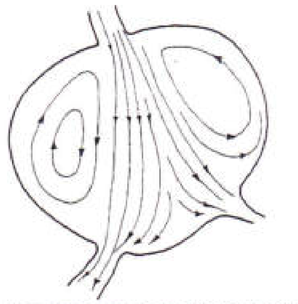

Figure 3: A schematic representation of flow within a cell of ceramic foam [7]

The objective of this work was to investigate the fluid flow in the channels of a CFF by using two new water model concepts.

Fundamentals

Under conditions of viscous flow, the flow of a Newtonian fluid through a porous medium obeys Darcy's Law [6]:

$$v_{sf} = -\frac{k}{\mu}\frac{\delta P}{\delta L} \qquad (1)$$

where: v_{sf} = superficial velocity
P = pressure
L = length of the filter medium
μ = the viscosity of the fluid
k = the permeability of the porous medium

In the case of laminar flow pressure drop will increase linearly with flow velocity. If the flow rate and thus the superficial velocity reaches a certain level, the inertial forces become more dominant and turbulent flow conditions start.

As the flow conditions inside the CFF can reach from regions of laminar flow to turbulent flow at a given flow rate, the filter can be regarded as a continuous reactor and the different volume fractions can be determined.

One important parameter for the characterisation of the fluid flow is the *average residence time* which is given by Equation 2 [9]:

$$\bar{t} = \frac{\textit{volume of fluid in the vessel}}{\textit{volumetric rate of fluid flow}} = \frac{V}{\dot{v}} \qquad (2)$$

Usually the residence time in reactors differs from the calculated residence time and a spread of different residence times can be found. This means that some fluid elements spend a longer and others a shorter period of time in the system.[9]. This distribution of residence times is an important characteristic and describes the performance of a reactor. According to the distribution of residence times one can define a wide spectrum of reactor types. One basic model is the so called *plug flow reactor*. In this kind of reactor all fluid elements have the same residence time. Another basic model is the *backmix* or *perfectly mixed reactor* where the fluid elements that enter the reactor instantaneously mix with the fluid elements that are already inside the reactor and the concentration of a given element is the same at any time or place in the reactor. In the so called *mixed model* it is assumed that the reactor volume is divided into fractions of *plug flow volume*, *backmix flow volume* and *dead volume* [9]

The residence time distribution of a fluid through a vessel can be determined by means of tracer techniques. There are several methods for introducing tracer material in a system. The two most important ones are [9]:

- Continuous addition of tracer (*step input*)
- Addition of a quantity of tracer over a short time interval (*pulse input*)

Pulse input of tracer involves the introduction of a quantity of tracer over a time period into the system. The tracer material must not interact with the fluid in the reactor or the reactor itself and the amount of tracer has to be negligible in comparison with the amount of fluid present in the system. In addition the time period over which the tracer is introduced to the system has to be very small compared to the calculated residence time [9]. The concentration of the tracer in the outlet stream is measured and plotted against time. The results can be plotted in dimensionless and therefore more general form by using the variables:

$$C = \frac{c}{Q/V} \tag{3}$$

where Q = quantity of tracer injected
V = volume of fluid in the vessel
C = dimensionless exit concentration

and

$$\Theta = \frac{t}{\bar{t}} \tag{4}$$

where: Θ = dimensionless time
t = actual time
$\bar{t}$ = average residence time

The results of pulse input tracer tests are plotted in the form of C against dimensionless time (C-Diagram). The area under each C curve must be unity since all the tracer introduced to the system must eventually leave the system [9]

$$\int_0^{\infty} C d\Theta \equiv 1 \tag{5}$$

According to the reactor type the C Diagrams have a typical design. The C diagrams for a plug flow volume, backmix volume and dead volume are shown in the following Figures.

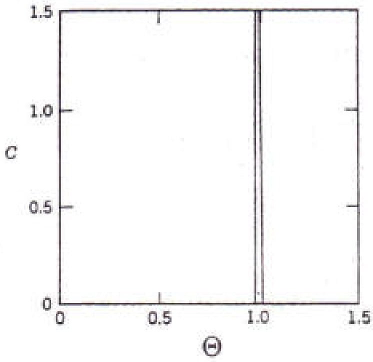

Figure 4: C diagram for Plug Flow V_p [9]

Plug Flow Volume

In the case of plug flow the tracer elements introduced to the system do not mix at all while they pass the reactor and arrive at the outlet exactly at $\Theta = 1$. So there is no spread of residence time.

Backmix Flow Volume

In a backmix flow reactor the tracer is dispersed immediately and uniformly throughout the system. This means the tracer concentration in the outlet stream is equal the concentration inside the reactor. Thus the C diagram shows during the test run a decrease in tracer concentration starting from unity. This means that a fraction of the tracer stays inside the system for a time much longer than the expected time while another fraction passes the system much quicker.

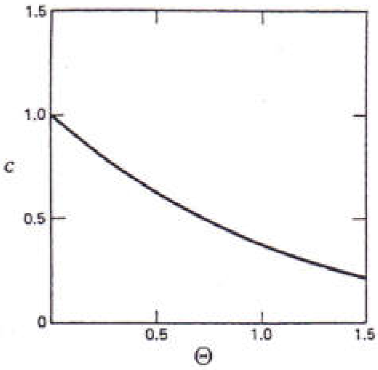

Figure 5: C diagram for backmix flow V_m [9]

Dead Volume

The presence of dead volume regions is indicated by a maximum in the C diagram at a time smaller than the average residence time and $C > 1$.

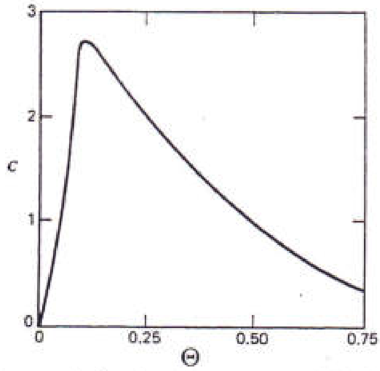

Figure 6: C Diagram indicating the presence of dead volume V_d [9]

While dead volume in the case of metallurgical reactors is not desirable, it is essential in filtration as only in dead volume regions the deposition of particles occurs. Thus this volume is better to be called "filtration volume" instead of dead volume for this special case.

Real reactors are usually a mixture of backmix flow, plug flow and dead fractions. It can be assumed that the plug flow fraction and backmix flow fraction are in series while the dead volume fraction is in parallel as illustrated in Figure **Error! Reference source not found.**

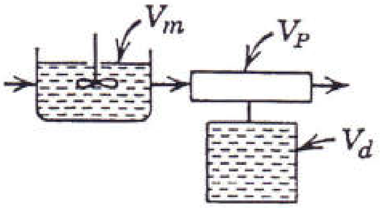

V_m: Mixing Volume
V_p: Plug Flow Volume
V_d: Dead Volume

Figure 7: Distribution of volume fractions [9]

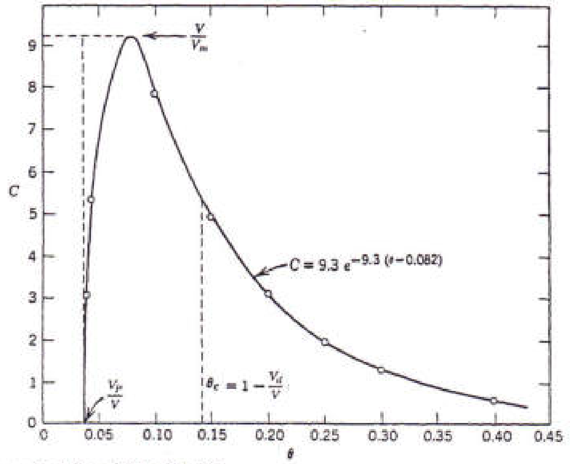

Figure 8: Mixed Model [9]

The C diagram for such a mixed model is shown in Figure 8. The volume fractions can be determined from the diagram.

The plug flow fraction can be found at the point of the diagram where a rapid increase in tracer concentration occurs according to Equation 6.

$$\Theta_p = \frac{t_p}{\bar{t}} = \frac{V_p}{V} \tag{6}$$

where: V = total volume
Θ_p = dimensionless time of increase in concentraion
t_p = absolute time of increase I concentration

For the determination of the dead volume fraction it is necessary to define the dimensionless actual mean residence time

$$\Theta_{mean} = \frac{\text{actual mean residence time}}{\text{calculated mean residence time}} = \frac{t_{mean}}{\bar{t}} \tag{7}$$

The dead volume fraction is then:

$$1 - \Theta_{mean} = \frac{V}{V_d} \tag{8}$$

Finally the backmix flow volume is:

$$V_m = V - V_d - V_p \tag{9}$$

Experimental setup

Full scale filter box model

The model used is shown in Figure 9. The full size 15", 17" or 20" Ceramic Foam Filter can be placed in the centre compartment of the model. In the model the water circulates in a closed loop during a given test time. The flow rate can be adjusted using a valve that controls the circulating pump. With a flow meter the flow rate can be controlled permanently [10].

Different models were constructed to demonstrate the flow behaviour in a single channel of a CFF as a function of flow rate. They consist of a row of connected spheres just like the pores of a CFF as to be seen in Figure 10. The relation between pore size and connecting channel was the same as pore size and window size in a CFF. In a CFF the window size is about a third of the pore size (see appendix). Furthermore the size of the models was big enough to visualise the flow using a tracer. A first model consisted of spherical pores. In real CFF's however the pores are elongated and thus a second model with elongated pores was tested. Finally the change in flow directions was considered, too, and a third model was constructed in which the liquid changed its flow direction several times, thus showing a certain tortuosity.

At the inlet of the models the tracer was added instantaneously. At the outlet an electrode was installed that measured the conductivity and thus the concentration of the tracer as a function of the running time. A valve at the outlet enabled different flow rates to be adjusted. The amount of water leaving the model in a defined time was measured and so the flow rate could be calculated.

A water reservoir connected by a tube with the inlet of the model ensured the same water level in the model for the whole running time. A tracer sulphuric acid was used; for visualisation of the flow $KMnO_4$ was added. The electric conductivity gives an immediate signal for every change in concentration.

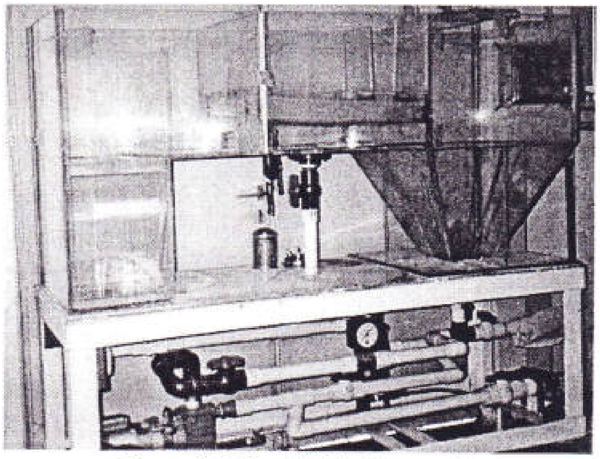

Figure 9: Full scale filter box model

Single channel model

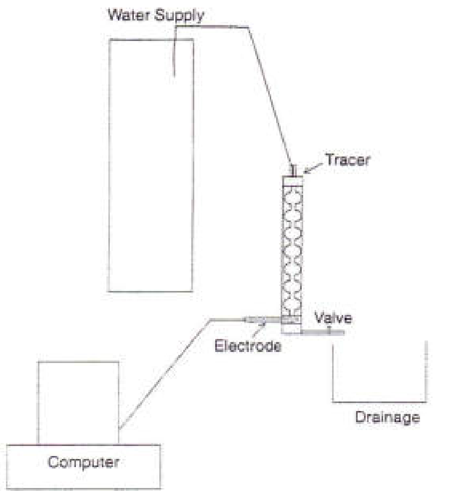

Figure 10: Single Channel Model with spherical pores

Test Programme

The full scale model was used to investigate the transient point from laminar to turbulent flow, indicated by the point where the flow rate-pressure drop diagram does not obey the Darcy Law anymore.

Also tracer tests were made. At different points of the surface of the filter $KMnO_4$ as tracer was added and the time measured until the first tracer appeared at the bottom of the filter. By this test it was also possible to find out if the filter shows the same flow behaviour all over its area.
With the single channel models the volume fractions as a function of flow rate could be determined.

Results

a) Pressure drop measurements
It was possible to determine the transient point from laminar flow to turbulent flow as a function of flow velocity and filter pore size for some filters. Figure 11 shows this behaviour for a 20"-filter. The transient point could be determined for a 65 ppi filter and a 80 ppi filter (1,0 cm/s and 1,15 cm/s) while for the other filters the flow velocity was not sufficient to reach the transient point.

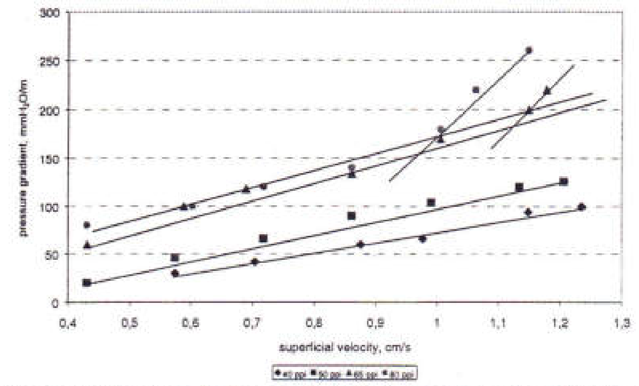

Figure 11: Pressure drop as a function of flow velocity and filter pore size

b) Full scale model tracer tests
Figure 12 shows the calculated residence time inside the filters.

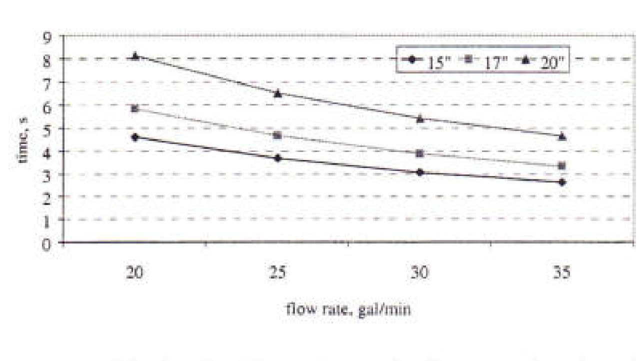

Figure 12: Calculated residence time in the filters as a function of flow rate

The results of the tracer measurements for a 20" filter can be seen in Figure 13.

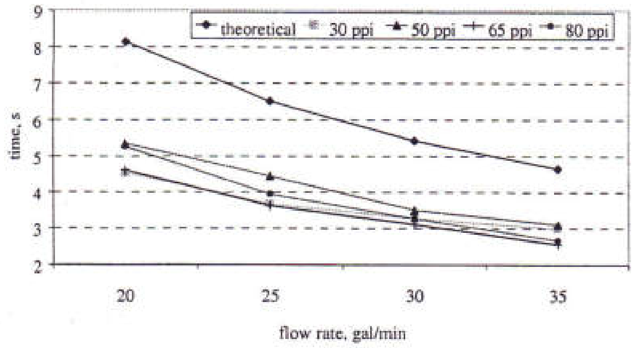

Figure 13: Measured residence time in a 20" filter

The results for the 17" and 15"filter showed the same behaviour. Generally the actual measured residence time is much shorter than expected. This indicates that there is a certain part of plug flow volume. The results of all the tests are shown in Figure 14 The plug flow part could be estimated by the differences between calculated and measured residence time. The other volume fraction must consist of the remaining volume (Figure 14)

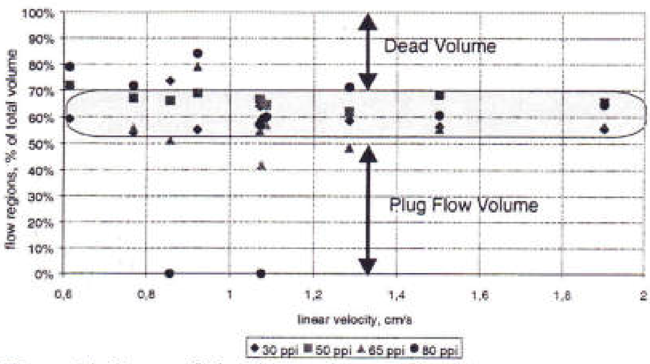

Figure 14: Range of plug flow volume of the filters

The tracer tests also showed how uniformly the residence times were spread over the area of the filter. Figure 15 shows that there is a uniform distribution over the area, however as the pore size becomes smaller there is more variation. The reason for this is not clear.

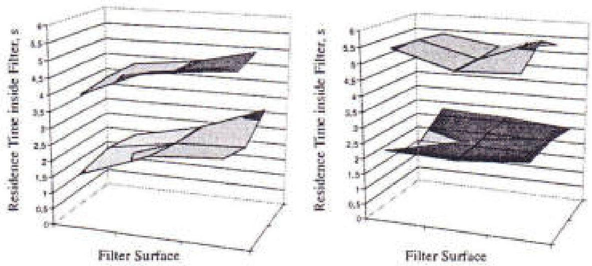

Figure 15: Distribution of residence times in a 20" 30 ppi filter (left) and a 80 ppi filter (right) at 20 gal/min and 35 gal/min

c) Single channel tracer tests
The C diagrams for each flow rate were evaluated and the different volume fractions determined. The results of these test could then be shown in the form of the following Figures. Calculations of similarity resulted in a minimum flow velocity of

0,177 mm/s and a maximum flow velocity of 1,6 mm/s as equivalent to the minimum and maximum flow velocities in the full scale model.

Model with spherical pores:

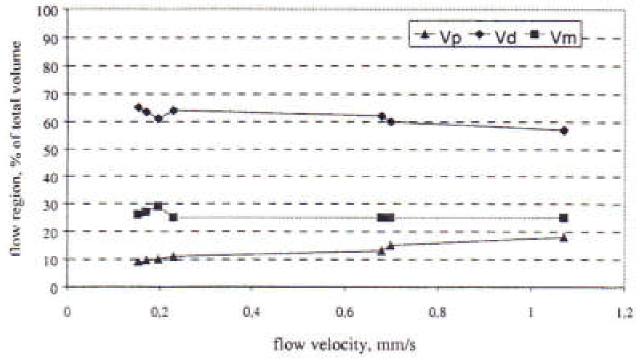

Figure16: Volume fractions as function of flow rate for model with spherical pores

The volume fractions could be determined and the influence of flow rate could be verified. Rising flow velocity led to more plug flow and less dead volume.

However as the pore shape of this model did not correspond to the pore shape of CFF's. A second model was tested with elongated pores.

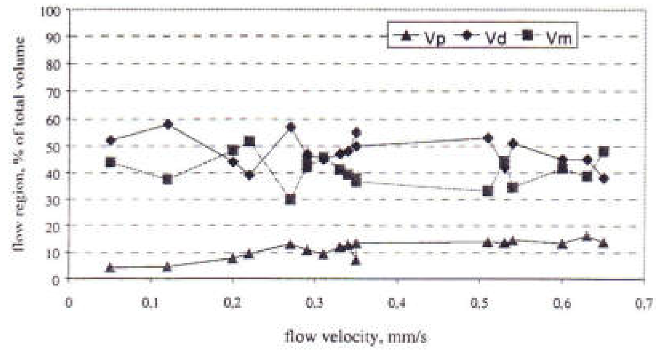

Figure 17: Volume fractions as function of flow rate for model with elongated pores

In this model the amount of filtration volume is smaller than in the model with spherical pores. At the same time the variation of the results is larger. Nevertheless the results are comparable to those in Figure 16

The third model that was tested finally considered the change in flow direction that the fluid experiences during its passage through the CFF. So a special designed tortuosity model was constructed. The behaviour of the volume fractions over a range of flow velocities (Figure 18) shows that in this model too the filtration volume is smaller than in the model with spherical pores.

As this model represents best the reality in a CFF it is likely that the filtration volume inside a CFF is about the same as found with this tortuosity model.

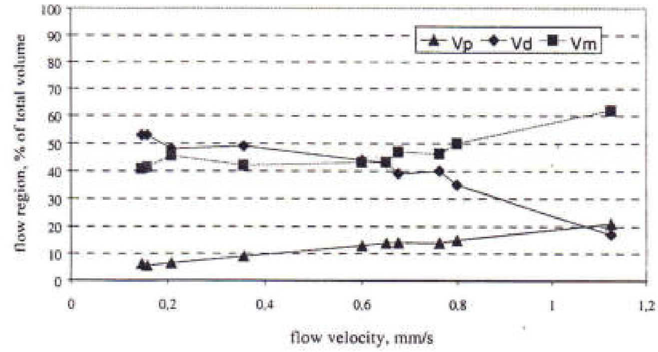

Figure 18: Volume fractions as function of flow rate for tortuosity model

While in the model with spherical pores the amount of dead volume was much higher than the amount of mixing volume, now both parts are similar up to a certain flow rate. Then mixing volume increases rapidly and dead volume decreases at the same time.

Conclusion

- The used single channel models showed an increase in mixing volume when flow velocity increased
- At the same time dead volume -which is essential for the deposition of particles- decreased.
- Also the shape of the pores was found to be very important. The amount of dead volume was higher if the pores were spherical.
- If the liquid changes its flow direction, the amount of dead volume is smaller and decreases more rapidly with flow rate.
- It could be shown that even at flow velocities which allow laminar flow, the filtration volume fraction decreased with increasing flow velocity.
- In good correlation to the measurements at the full scale model, in the single channel model tests the presence of dead volume and plug flow volume could be verified.

Appendix

Calculations of similarity between full scale filtration box model and single channel models.

a) Pore and window sizes in CFF's

	dpore, µm	dwindow, µm
30 ppi	1900	636
50 ppi	1045	363
60 ppi	818	318
70 ppi	727	272
80 ppi	681	227

b) linear velocities as a function of filter size and flow rate

Filter size, inch	Flow rate, gal/min	linear velocity, mm/s
15 "	20	14,5
	35	25,4
17"	20	11
	35	19,3
20"	20	7,8
	35	13,6

c) Boundary conditions

v_{min}, mm/s	7,8
v_{max}	25,4
d_{min}, mm	0,681
d_{max}	1,9

d) Similarities

$N_{ReCFF} = N_{Re\,mo}$

$v_{Mo} = (d_{CFF} * v_{CFF})/d_{Mo}$

$\Rightarrow v_{momax} = d_{CFFmax} * v_{CFFmax}/d_{Mo}$

also: $v_{max} = 1,6$ mm/s

$V_{min} = 0,177$ mm/s

References

[1] Dupuis, C.; Beland, G.; M Martin J.-P. "Filtration Efficiency of Ceramic Foam Filters for Production of High Quality Molten Aluminium Alloys" 32nd Annual Canadian Conference of Metallurgists, 29th August – 2nd September 1993

[2] Desmoulin, J.-P. "Reliability of molten metal filtration" Light Metals 1992, pp. 1093-1099

[3] Eckert, C. E.; Miller, R. E. "Molten Metal Filtration: Fundamentals and Models" Light Metals 1984, pp. 1281-1304

[4] Gaukler, L. J.; Waeber, M. M.; Conti, C. et al. "Industrial Application of Open Pore Ceramic Foam for Molten Metal Filtration" Light Metals 1985, pp. 1261-1283

[5] Keegan, N.; Collum, J.M. "Depth of ceramic foam filters vs. filtration efficiency" Light Metals 1992, pp. 1086-1091

[6] Tian, C.; Guthrie R.I.L.; "Rheological Aspects of Liquid Metal Filtration using Reticulated Ceramic Foam Filters" Light Metals 1993, pp. 1003-1007

[7] Apelian, D.; Mutharasan, R.; Romanowski, C.A. "Commercially Available Porous Media for Molten Metal Treatment"; Light Metals 1982, pp. 935-967

[8] Themelis N. "Transport and chemical rate phenomena"; Gordon and Breach Publishers, 1995

[9] Szekely, J.; Themelis, N.; "Rate Phenomena in Process Metallurgy"; Wiley-Interscience, 1971

[10]Mills, T. J.; McCollum, J. M. "Water Model Filtration Efficiency Studies of Ceramic Foam Filters" Light Metals 1994, pp. 1001-1005